**Helmholtz-Zentrum Dresden-Rossendorf (HZDR)**

# Effect of anisotropic microstructure of ODS steels on small punch test results

Altstadt, E.; Bergner, F.; Das, A.; Houska, M.;

# Accepted Manuscript

Effect of anisotropic microstructure of ODS steels on small punch test results
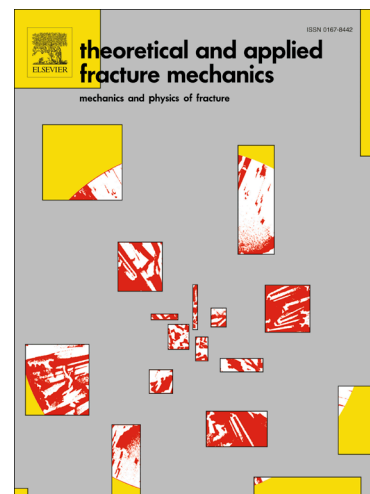
E. Altstadt, F. Bergner, A. Das, M. Houska

# Effect of anisotropic microstructure of ODS steels on small punch test results

E. Altstadt [1,]*, F. Bergner [1], A. Das [1] and M. Houska [1]

[1] Helmholtz-Zentrum Dresden-Rossendorf, Germany

* Correspondence: e.altstadt@hzdr.de; Tel.: +49-351-260-2276

**Abstract:** Hot rolling and hot extrusion of oxide-dispersion strengthened (ODS) ferritic steels give rise to anisotropic microstructures and mechanical properties and may provoke related phenomena such as secondary cracking. In this study, we consider the small punch (SP) test – a method, applicable in the case of small amounts of available material and well established for isotropic materials. The SP test was applied to investigate the effect of sample orientation on deformation and cracking for one hot-rolled and two hot-extruded ODS ferritic steels. Existing microstructural evidence is used to rationalize the observed anisotropic fracture behaviour. The SP test results are compared with those from existing fracture mechanics tests based on sub-sized C(T) samples. The applicability of the empirical conversion of SP-based into Charpy-based transition temperatures is evaluated. The fractographic manifestation of load drops in SP load-displacement curves is identified and the analogy to secondary cracking in fracture mechanics tests is shown.

## 1. Introduction

Oxide dispersion strengthened (ODS) steels are candidate materials for fuel claddings of Gen-IV sodium cooled fast reactors as well as for the first wall and blanket structures of fusion reactors [1–3]. The envisaged operation temperature is up to 650 °C. The focus of ODS materials development was put on superior creep and swelling properties. However, sufficient tensile and fracture mechanical properties are required for safety relevant structural applications in the whole range from room to operation temperature. Lindau et al. demonstrated that yield stress and ultimate tensile stress (UTS) of ODS Eurofer are significantly higher in comparison to the non-ODS counterpart for temperatures up to 750 °C [4]. The creep resistance at 750 °C is also significantly improved. However, the ductile-to-brittle transition temperature (DBTT) was found to be significantly higher than that of non-ODS Eurofer [4]. Chaouadi et al. [5] found a significant crack resistance degradation of ODS Eurofer at increasing test temperature. In particular, at 550 °C and 650 °C, the crack resistance is very low. Byun et al. [6] have demonstrated that high temperature fracture toughness could be significantly improved by appropriate thermo-mechanical treatments.

The fracture behaviour of ODS materials is governed by grain morphology. Chao et al. [7] found a grain size anisotropy for a 20Cr ODS alloy manufactured as a tube by hot rolling. The grains were found to be elongated along the rolling direction. Small Specimen (KLST) impact tests and subsequent EBSD analyses of the crack region revealed intergranular cracks along

the elongated grain boundaries which constitute weak interfaces. The term "delamination" originating from laminated composite materials was adopted for this type of intergranular cracking. The delamination phenomenon had earlier been reported for ultrafine grain structure steels by Kimura et al. [8]. Depending on the orientation of the weak planes in the impact specimen, they discriminated a "crack arrester" and a "crack divider" situation. The impact of two different fabrication routes (hot rolling and hot extrusion) on the grain morphology and thereby on the fracture behaviour in different orientations was investigated in detail by Das et al. [9,10].

The small punch (SP) test has long been accepted as a method to estimate mechanical properties from small quantities of materials. In particular the ductile-to-brittle transition temperature, the yield stress, the ultimate tensile stress and creep strength can be extracted for homogeneous and isotropic metals [11–19]. The SP test is not intended as a general replacement of conventional tests such as tensile tests, Charpy impact tests or fracture mechanics testing. The SP test is especially useful in one or more of the following cases [17]: (i) the available amount of material is limited, (ii) the material is highly activated by neutron or proton irradiation, (iii) material properties are non-homogeneous and exhibit significant gradients. Therefore it is generally useful to include this technique in the characterization of ODS alloys. Case (i) was the reason to use the SP test in this work.

So far, the effect of the above mentioned anisotropic microstructure on SP test results has only rarely been investigated [20,21]. A systematic comparison of the fracture behaviour in SP tests, Charpy impact tests and fracture mechanics tests is needed to understand the meaning of SP based DBTTs in dependence on specimen orientation. In this paper we investigate one hot-rolled and two hot-extruded ODS steels by means of SP testing. The paper aims at relating features of SP force-displacement curves and SP based DBTTs to fracture mechanisms depending on grain morphology and orientation. In particular, we put the focus on load drops in the load-displacement curves (pop-ins) and their corresponding microstructural and fractographic features. The SP results are discussed in the view of existing fracture mechanics tests for the same materials. We investigate the effect of the consideration and non-consideration of pop-ins in the energy based DBTT evaluation.

## 2. Materials and Methods

Three different ODS steels were selected for testing, one hot-rolled and two hot-extruded. The denomination in this paper is ODS-HR, ODS-HE1, ODS-HE2.

**ODS-HR** is a 13%Cr ODS steel hot-rolled plate provided by Karlsruhe Institute of Technology, Germany (KIT). The main production steps include: mechanical alloying in an attritor ball mill, encapsulation of the powder, hot isostatic pressing at 1100 °C and 100 MPa and rolling at 1100 °C from a diameter of 80 mm to a plate of 7 mm thickness in 5 runs [9,22].

**ODS-HE1** is a hot-extruded 13% Cr ODS steel round bar also provided KIT. The main fabrication steps include: mechanical alloying in an attritor ball mill, encapsulation of the powder, evacuation of the capsule and hot extrusion at 1100 °C [10,22]. Same primary powder batch as ODS-HR.

**ODS-HE2** is a hot-extruded 14% Cr ODS steel round bar provided by Centro Sviluppo Materiali, Italy (CSM). Gas atomized pre-alloyed steel powder was mixed with 0.3% $Y_2O_3$ and dry ball milled in an environment of Ar and H. After canning, direct hot extrusion was performed at 1150 °C with an extrusion ratio of 22.5. A heat treatment at 1050 °C was applied for one hour with subsequent cooling in the furnace [23,10].

The bulk chemical composition of the materials is given in Table 1. The microstructure of the investigated ODS steels is characterized by fine and coarse grained regions. In the hot-rolled material ODS-HR the coarse grained regions exhibit elongated pan-cake shaped grains with the longest dimension parallel to the rolling direction L and the second longest dimension parallel to the transverse direction T [9] (cf. Fig. 1a), whereas in the hot-extruded materials ODS-HE-1 and ODS-HE-2, cigar shaped grains elongated along the extrusion direction L were observed [10] (cf. Fig. 1b).

**Table 1.** Chemical composition of the tested ODS steels (wt%) [10,22]

| Material | C | Si | P | Ti | Cr | Ni | W | $Y_2O_3$ * |
|---|---|---|---|---|---|---|---|---|
| ODS-HR | 0.028 | 0.051 | 0.01 | 0.138 | 12.99 | 0.101 | 1.01 | 0.3 |
| ODS-HE1 | 0.028 | 0.051 | 0.01 | 0.138 | 12.99 | 0.101 | 1.03 | 0.3 |
| ODS-HE2 | 0.010 | 0.371 | 0.006 | 0.238 | 13.76 | 0.239 | 0.84 | 0.3 |

* Nominal $Y_2O_3$ content of the powder composition



**(a)**                    **(b)**

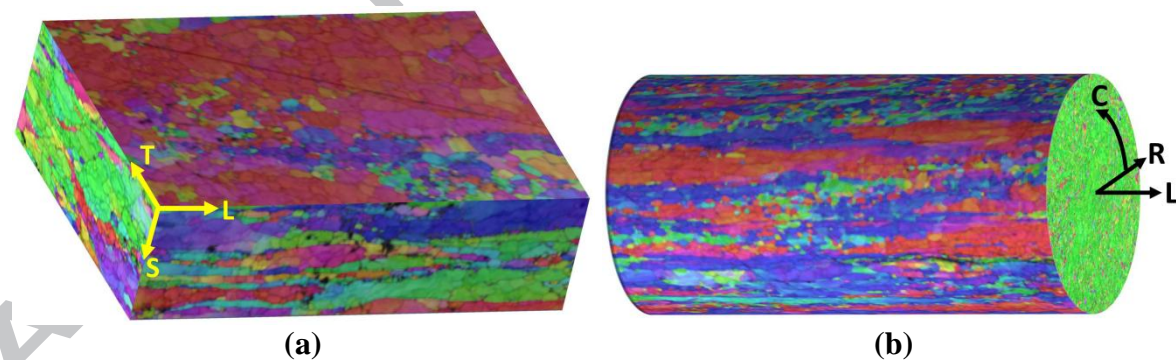**Figure 1**. EBSD images from [9,10]: (a) pan-cake shaped coarse grains in ODS-HR; (b) Cigar shaped coarse grains in ODS-HE-1.

Mechanical properties are listed in Table 2. The KLST based DBTT of ODS-HR in Table 2 is an estimation based on 5 KLST impact tests [22]. The conversion to standard Charpy DBTT gives $T_{CVN} \approx$ -5°C according to the correlation $T_{CVN} = T_{KLST} + 65\,K$ established by Klausnitzer [24].

**Table 2.** Mechanical properties of the tested ODS steels at room temperature [9,10,22] orientation L

| Material | Yield stress | Ultimate tensile stress | Total elongation | DBTT-KLST (LS) |
|---|---|---|---|---|
| ODS-HR | 664 MPa | 777 MPa | 26.6% | $\approx$ -70 °C |
| ODS-HE1 | 928 MPa | 1041 MPa | 24.5% | -- |
| ODS-HE2 | 760 MPa | 977 MPa | 21.1% | -- |

Small punch tests were executed in three orientations for ODS-HR (S - thickness direction, L - rolling direction and T - transverse direction) and in two orientations for ODS-HE-1 and ODS-HE-2 (L - extrusion direction, R/C - radial/circumferential direction). The orientation refers to the normal direction of the specimens. In case of ODS-HE1 and ODS-HE2, it is justified to assume that the directions R and C are equivalent because of the axial symmetry of the extrusion process. Moreover, plane samples cut from a round bar in axial direction always exhibit a combination of R and C orientation for geometrical reasons. As the stress components in thickness direction of a small punch sample are much smaller than the in-plane stress components, the S oriented specimens represent the mechanical behaviour of the LT plane, the T oriented specimens those of the LS plane and the L oriented specimens those of the TS plane [21].

Specimens of 10 x 10 x 0.5 mm (8 x 8 x 0.5 mm in case of ODS-HR) were manufactured by electrical discharge machining and subsequent grinding to final thickness with grit 2500. The maximum accepted thickness tolerance was $\pm$5 μm. The thicknesses of all specimens were measured by laser micrometer with an accuracy of $\pm$1 µm. Specimens with a thickness outside the tolerance were not used. The main parameters of the SP set-up are: punch diameter $d$ = 2.5 mm, receiving hole diameter $D$ = 4 mm, receiving hole edge radius $R_E$ = 0.5 mm (cf. Fig. 2). The edge size is larger than proposed in the upcoming standard [25]. While the effect of the edge size on the estimation of tensile properties (in particular the yield stress) is significant, it can be neglected for the estimation of the ductile-to-brittle transition temperature [17]. The punch displacement $v$ was measured by an inductive sensor with an accuracy of $\pm$1 μm and corrected for the device compliance. The punch force was measured by means of a load cell placed between the puncher and the cross head of the testing machine with an accuracy of $\pm$5 N. In total a number of 168 tests were performed. The temperature range was from -188 °C to +350 °C. The subsequent fractographic analysis of selected tested SP specimens was done by SEM using a Zeiss EVO 50 device.
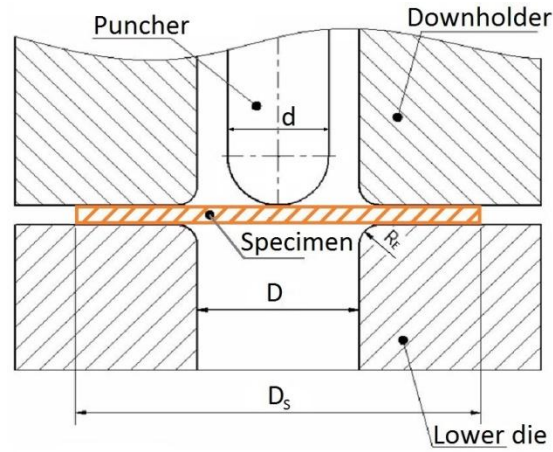
**Figure 2**. Geometry of the SP set-up

The SP based ductile-to-brittle transition temperature $T_{SP}$ is determined on the basis of normalized energies $E_n = E_{SP}/F_m$ of the different tests [26]. $E_{SP}$ is the area under the force-displacement curve up to the displacement $v_m$ at maximum force $F_m$:

$$E_{SP} = \int_0^{v_m} F(v)dv \approx \sum_{k=2}^{kmax} \frac{F_k + F_{k-1}}{2} \cdot (v_k - v_{k-1}) \tag{1}$$

A tanh-fitting procedure was applied for the $E_n(T)$ dependence based on the following equation:

$$E_n(T) = A + B \cdot \tanh\left[\frac{T - T_{SP}}{C}\right] \tag{2}$$

A least square fitting procedure was used to determine the coefficients $A$, $B$, $C$, and $T_{SP}$. This procedure includes a statistical error estimation for the fit parameters [27]. The Charpy transition temperature $T_{CVN}$ can be recalculated by the well-known correlation $T_{SP} = \alpha \cdot T_{CVN}$ (temperatures in K) [14]. For our set-up we used $\alpha = 0.43$ [17]. This value was further validated for a number of ferritic-martensitic steels and reactor pressure vessel steels. However, these results are not yet published.

In case of discontinuous load drops (pop-ins) in the force-deflection curve, caused by crack initiation and subsequent crack arrest [21], the procedure for the energy calculation Eq. (1) is modified so that $v_m$ and $F_m$ are replaced by displacement $v_{1p}$ and force $F_{1p}$ of the first significant pop-in (cf. Fig. 3). A load drop is considered as significant, if $\Delta F/F_m \geq 0.05$.
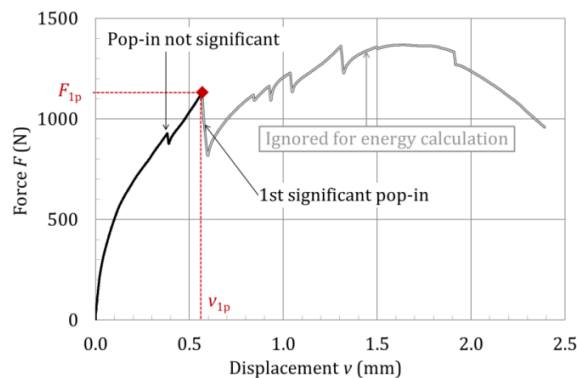
**Figure 3**. Energy calculation in case of load-drops

This procedure is established in the upcoming European SP test standard [25], with the exception that the criterion for the significance of a pop-in is $\Delta F/F_m \geq 0.1$ in [25]. We used the more sensitive criterion based on the insight that also smaller pop-ins manifest themselves clearly in fractography results (cf. section 3.3). For comparison, the $E_n(T)$ dependence was also calculated ignoring the pop-ins, i.e. integrating the $F(v)$ curves up to $v_m$ even though significant pop-ins are present.

## 3. Results

### 3.1. Force-displacement curves

Selected force-displacement curves are shown in Figs. 4-6. For the hot-rolled material ODS-HR, there are significant differences between the orientations L and T on the one hand and orientation S on the other hand. The maximum forces $F_m$ and corresponding displacements $v_m$ are smaller in L- and T-oriented samples as compared to S-oriented samples. Moreover, load-drops (pop-ins) are observed at low test temperatures (below -70 °C) for orientations L and T but not for orientation S. For room temperature, the parameters $v_m$ and $F_m$ are summarized in Table 3. It is interesting to note that the pop-ins are accompanied by audible acoustic emissions.

For the hot-extruded materials, pop-ins do not occur in either orientation. The maximum forces $F_m$ and corresponding displacements $v_m$ are slightly smaller in C/R oriented samples as compared to orientation L. There is, however, a pronounced difference between the two materials ODS-HE1 and ODS-HE2 in that the latter one exhibits significantly lower absolute values. This is related to the considerably higher yield stress and tensile strength of ODS-HE1 (cf. Table 2).

Unstable fracture at displacements between 0.5 and 1 mm is observed for all hot-rolled and hot extruded materials at very low test temperatures. The associated $F(v)$ curves do not exhibit pop-ins nor a stable load decrease beyond $F_m$ (Figures 4-6).
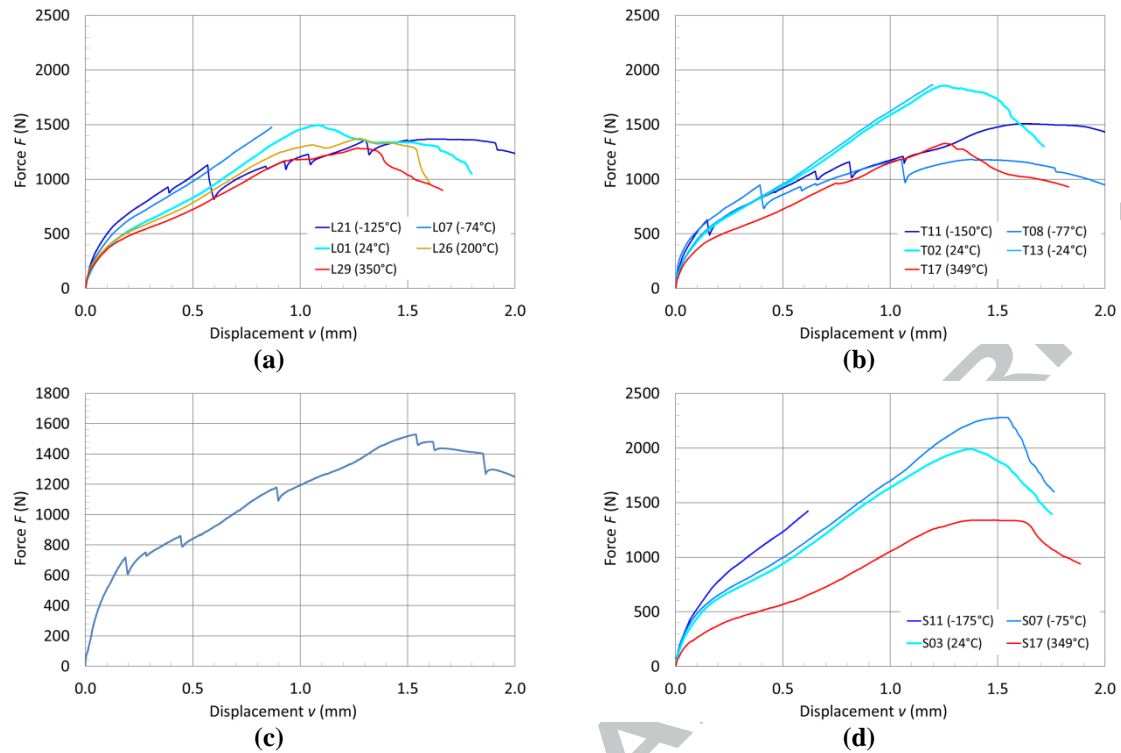
**Figure 4**. Force-displacement for material ODS-HR; (a) orientation L; (b) orientation T; (c) sample T10 tested at -150 °C (orientation T); (d) orientation S
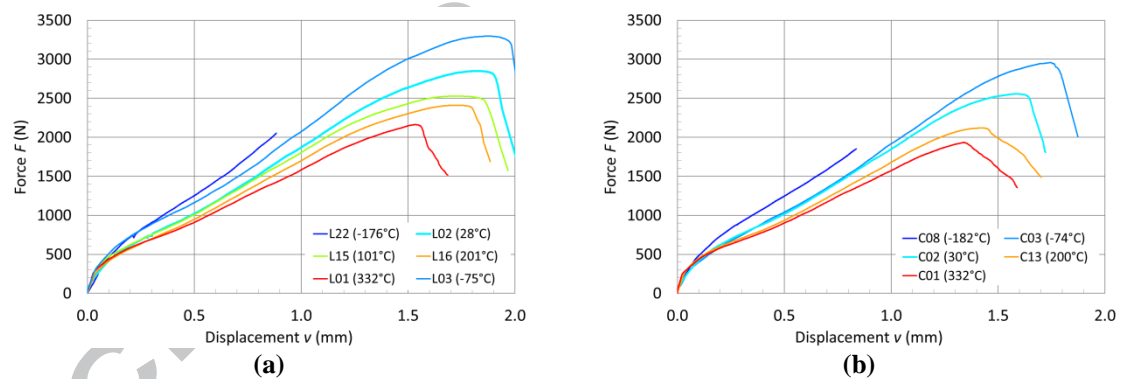


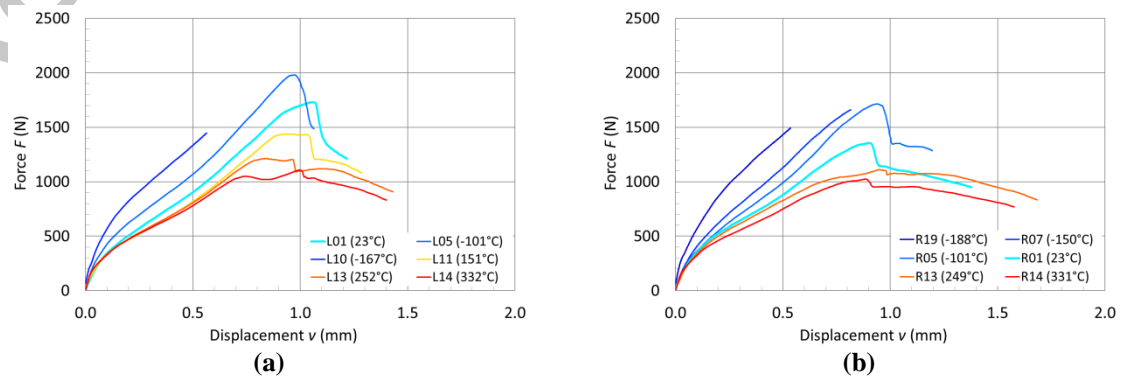**Figure 5**. Force-displacement for material ODS-HE1; (a) orientation L, (b) orientation C/R



**Figure 6**. Force-displacement for material ODS-HE2; (a) orientation L, (b) orientation C/R

**Table 3.** Parameters of the force-displacement curves at room temperature

| Material Orientation | ODS-HR L | ODS-HR T | ODS-HR S | ODS-HE1 L | ODS-HE1 C/R | ODS-HE2 L | ODS-HE2 C/R |
|---|---|---|---|---|---|---|---|
| $v_m$ (mm) | 1.08 | 1.26 | 1.37 | 1.82 | 1.59 | 1.05 | 0.90 |
| $F_m$ (N) | 1494 | 1857 | 1991 | 2848 | 2556 | 1730 | 1355 |

## 3.2 Ductile-to-brittle transition temperatures

The SP ductile-to-brittle transition temperatures were determined for all materials and orientations as described in section 2. In case of pop-ins, the energy calculation was based on the $F(v)$ curve up to the first significant pop-in (cf. Fig. 3). This was only relevant for the material ODS-HR in the orientations L and T. The dependences of the normalized SP energy $E_n$ on temperature are shown for all materials in Figs. 7-9. The definition of $E_n$ is given in section 2. The SP transition temperatures $T_{SP}$ and the corresponding Charpy transition temperature $T_{CVN}$ (converted from $T_{SP}$) are listed in Table 4. The statistical error analysis for the estimation of $T_{SP}$ yielded uncertainties of $|\Delta T_{SP}| \leq 11$ (ODS-HR and ODS-HE-2) and $|\Delta T_{SP}| \leq 4$ (ODS-HE-1).
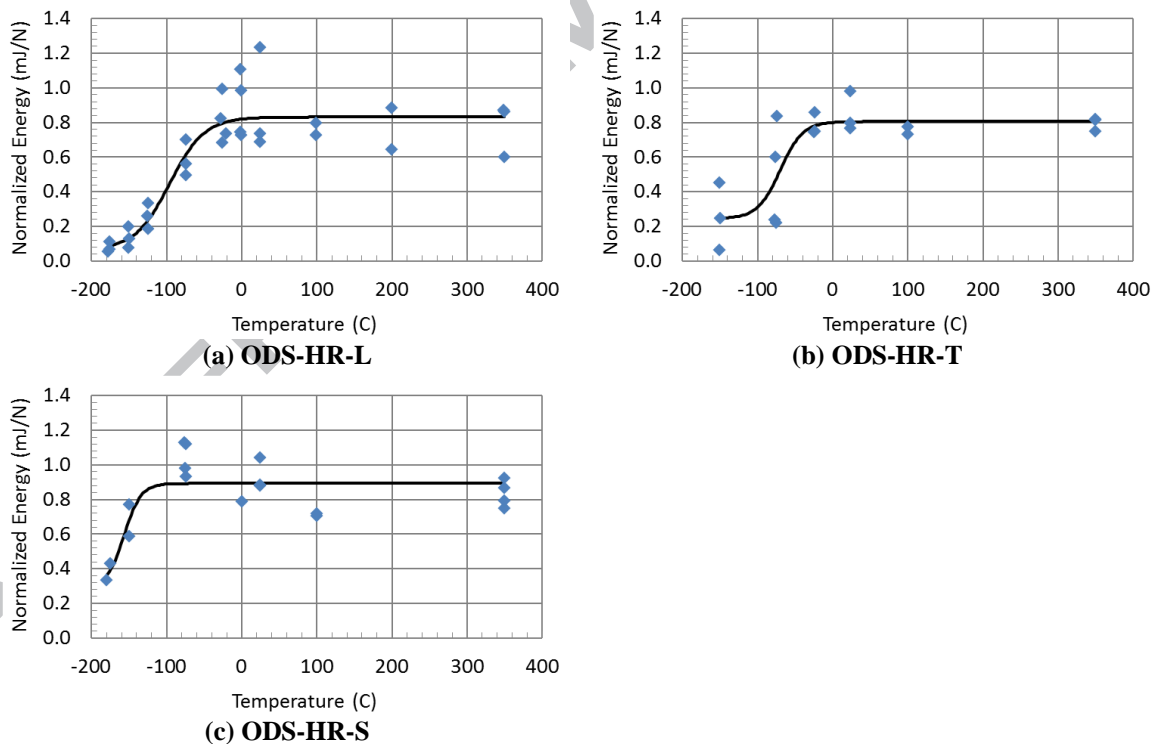


**(a) ODS-HR-L**

**(b) ODS-HR-T**

**(c) ODS-HR-S**

**Figure 7**. $E_n(T)$ fit curves for ODS-HR: **(a)** orientation L, $T_{SP} = -96$ °C; **(b)** orientation T, $T_{SP} = -70$ °C; **(c)** orientation S, $T_{SP} = -157$ °C
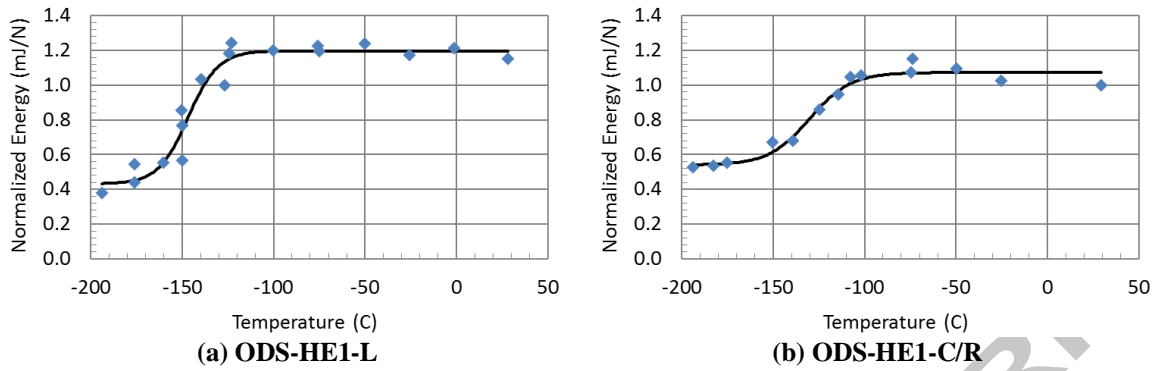
**(a) ODS-HE1-L**



**(b) ODS-HE1-C/R**

**Figure 8**. $E_n(T)$ fit curves for ODS-HE1: **(a)** orientation L, $T_{SP}$ = -147 °C; **(b)** orientation C/R, $T_{SP}$ = -130 °C



**(a) ODS-HE2-L**



**(b) ODS-HE2-C/R**
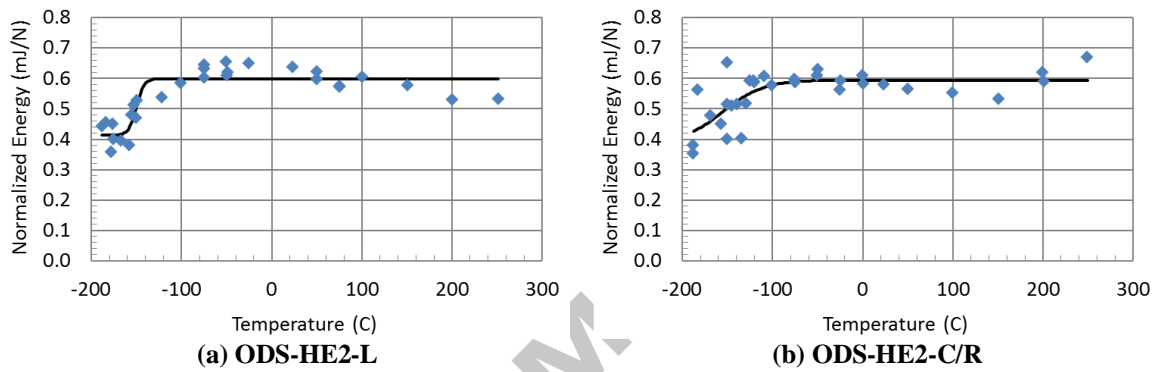
**Figure 9**. $E_n(T)$ fit curves for ODS-HE2: **(a)** orientation L, $T_{SP}$ = -150 °C; **(b)** orientation C/R, $T_{SP}$ = -154 °C
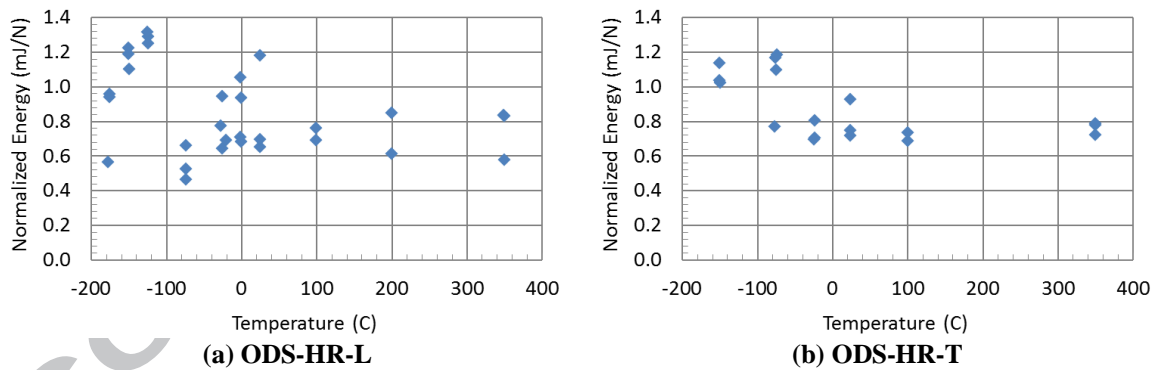


**(a) ODS-HR-L**



**(b) ODS-HR-T**

**Figure 10**. Temperature dependent normalized energies $E_n$ for ODS-HR with neglected pop-ins: **(a)** orientation L; **(b)** orientation T

**Table 4.** Ductile-to-brittle transitions temperatures

| Material Orientation | ODS-HR L | ODS-HR T | ODS-HR S | ODS-HE-1 L | ODS-HE-1 C/R | ODS-HE-2 L | ODS-HE-2 C/R |
|---|---|---|---|---|---|---|---|
| $T_{SP}$ (°C) | -96 | -70 | -157 | -147 | -130 | -150 | -154 |
| $T_{CVN}$ (°C) * | +139 | +199 | -2 | +21 | +59 | +13 | +4 |

* Recalculated from: $T_{SP}$[K] = 0.43·$T_{CVN}$[K]

Figure 10 shows the normalized SP energies as a function of temperature for the case that significant pop-ins in the $F(v)$ curve are neglected for the energies calculation (Eq. 1). The relevant $F(v)$ curves of ODS-HR for L and T oriented samples were integrated up to $v_m$

regardless of the occurrence of pop-ins. In this case a ductile-to-brittle transition is not existing in $E_n(T)$ dependency. A tanh-fit and hence the determination of $T_{SP}$ is not possible.

### 3.3 Fractographic analysis

Figure 11 shows the fractographic analysis of a SP sample from ODS-HR, orientation T, tested at -150 °C. The main crack has a radial orientation and is located in the LT plane. Several liftings (flakes) can be observed. The fracture surface is predominantly characterized by cleavage with some ductile areas (Fig. 11b). Underneath the flakes, the fracture is completely cleavage without ductile elements (zone 2, Fig. 11c). The corresponding force-displacement curve is shown in Fig. 4c. The number of pop-ins (7) corresponds approximately to the number of visible flakes in Fig. 11a. For the size of all pop-ins $\Delta F/F_m < 0.1$ holds.
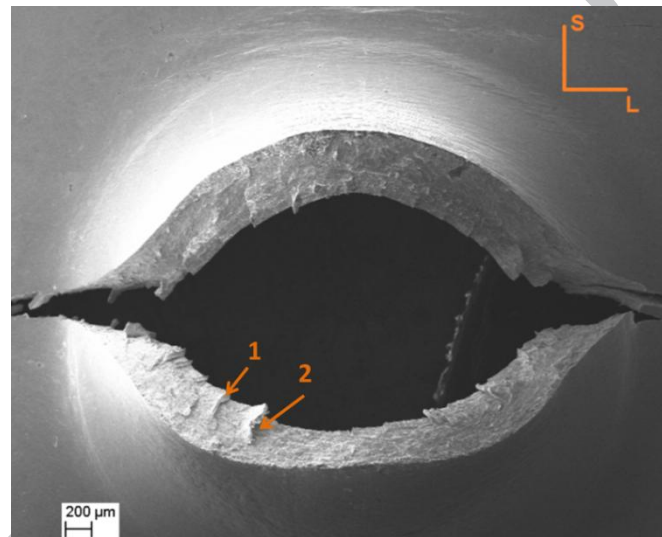


**(a)**
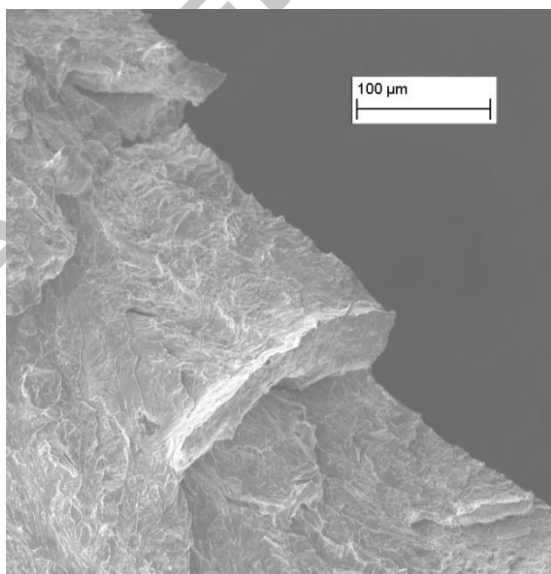


**(b)**



**(c)**

**Figure 11**. SEM pictures of the fracture surface of sample T10 from ODS-HR tested at -150 °C: (a) overview; (b) magnification of zone 1; (c) magnification of zone 2, tilted by 40°, underneath the flake
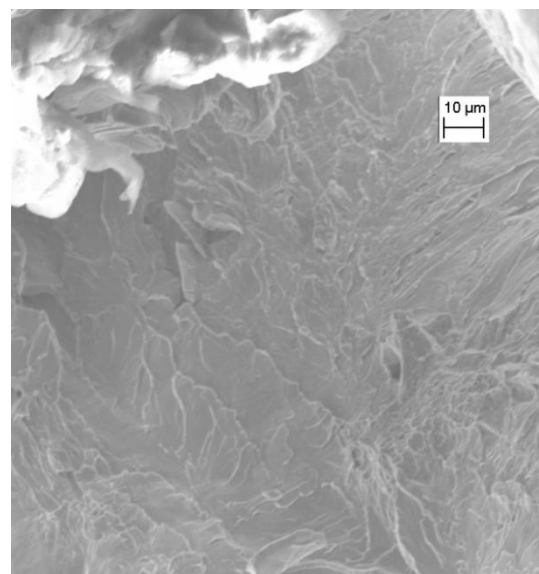
Figure 12 shows the fractographic analysis of a SP sample from ODS-HR, orientation S, tested at +100 °C. The main crack exhibits a fish-mouth-like circumferential shape. Thus it is not located in a specific plane. The fracture appearance is fully ductile. However, some secondary cracks in the LT plane were found (Fig. 12c).



**(a)**



**(b)**



**(c)**
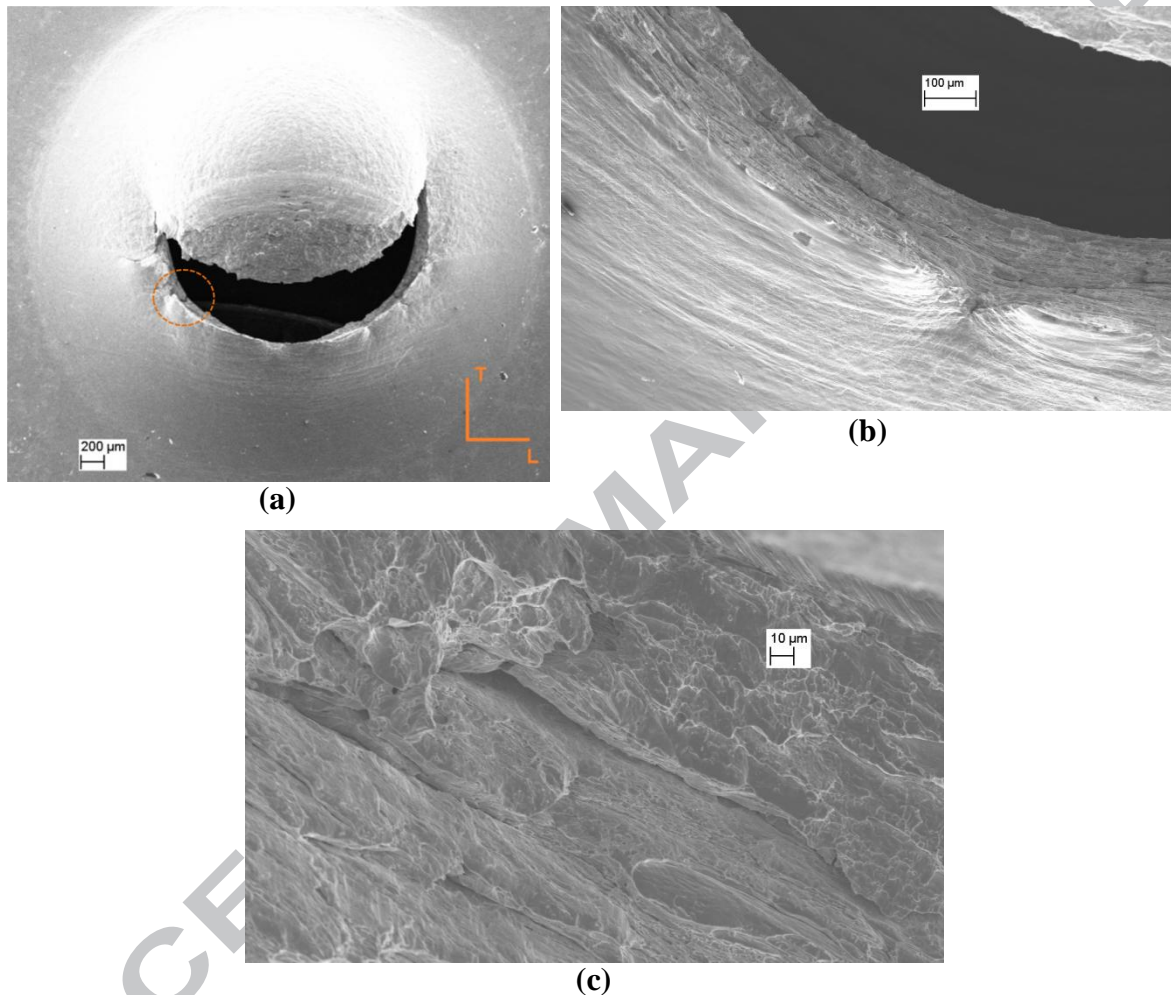
**Figure 12**. SEM pictures of the fracture surface of sample S05 from ODS-HR, tested at +100 °C: (a) overview; (b) magnification of the encircled zone; (c) further magnification of image b tilted by 39°

For the hot-extruded material ODS-HE2, the shapes of the fractures are similar to those of the hot-rolled materials, i.e. radially oriented for low temperatures (below -100 °C) and with a circular shape for higher temperatures. However, lifting (flakes) could not be observed for any testing temperature and orientation.

## 4. Discussion

### 4.1 The origin of pop-ins

As reported in section 2, the investigated ODS steels exhibit an anisotropic microstructure with fine and coarse grained regions and pan-cake shaped (ODS-HR) or cigar shaped (ODS-

HE-1, ODS-HE-2) elongated grains (Fig. 1). In particular, the hot-rolled material exhibits a {100}<110> crystallographic texture [28]. This means that for the majority of grains their {100} plane is parallel to the rolling plane LT and that their <110> direction is parallel to the rolling direction L. In the hot-extruded materials there is a texture where the <110> directions of the grains are parallel to the extrusion direction L, but without a preferred orientation of the {100} planes [28].

It was reported that, in the hot-rolled material, the crack resistance is higher in the coarse grained regions as compared to the fine grained regions [9]. Thus the crack growth in thickness direction S is hindered due to the pancake shaped morphology of the coarse grains. Moreover, the above mentioned crystallographic texture promotes an easier cracking in the LT plane (perpendicular to the thickness direction S) as compared to the other planes. The microstructural features responsible for these weak zones are discussed in detail in [9,28].

The weak zones lead to delamination-like failures under tensile stress in S direction [9,21,28] and gives rise to pop-ins in the $F(v)$ curves of L and T oriented SP samples. The fracture process is characterized by an interplay of stable transgranular crack growth and unstable cracking in the weak zones along the LT planes. Unstable cracking events are also assumed to be responsible for the mentioned audible acoustic emissions. Crack arrest occurs when the crack tip arrives at coarse grains which are extended perpendicularly to the crack propagation direction. The fracture in the SP specimen is preferentially oriented in radial direction (LT plane, i.e. perpendicular to the S direction) and the fracture surface exhibits flakes (cf. Fig 10a). Their formation can be associated with the pop-ins in the $F(v)$ curves. By contrast, such a mechanism does not exist in S oriented samples as the weak zones are not loaded in tension.

In hot-extruded materials, the coarse grains are extended only in one direction (L). Thus the SP samples are less susceptible to unstable cracking and subsequent crack arrest for pure geometrical reasons. Consequently pop-ins cannot be observed in the $F(v)$ curves.

In fracture mechanics investigations by means of 0.25C(T) compact tension samples, it was found that the ODS-HR material is susceptible to secondary cracking, i.e. cracks in planes perpendicular to main crack plane were observed [9,28]. By contrast, the hot-extruded materials ODS-HE1 and ODS-HE2 were found to be unsusceptible to secondary cracking [10,28]. In Fig. 13 two examples of load-displacement curves for the hot-rolled material are shown. The curves also exhibit load drops. The analysis of the complete fracture mechanics data set showed that the presence of secondary cracks is a necessary precondition for the load drops. The load drops were observed for ODS-HR at test temperatures up to +100 °C.
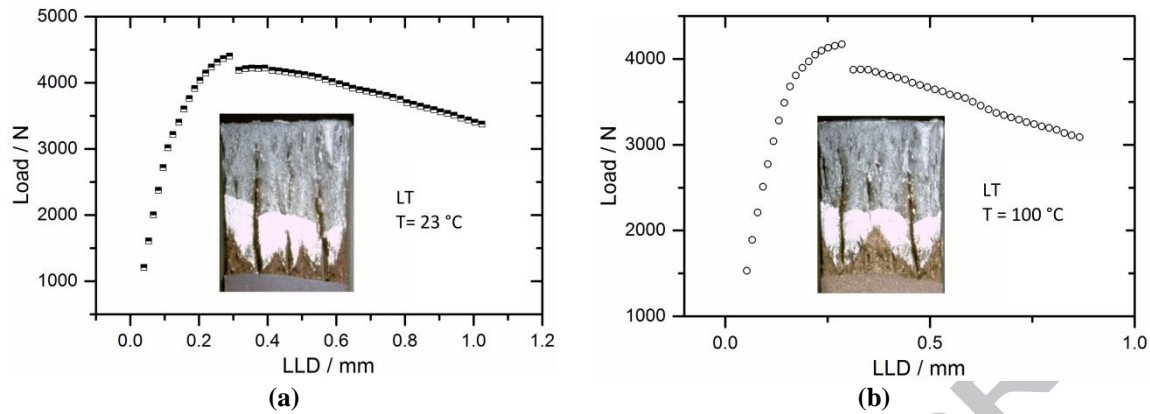
**Figure 13**. Fracture mechanics tests of ODS-HR with 0.25 C(T) specimens (LT orientation); Load vs. load line displacement (LLD); **(a)** room temperature; **(b)** T = 100 °C.

Apparently, the occurrence of pop-ins in the SP $F(v)$ curves and associated flakes at the fracture surfaces correspond with the occurrence of load drops in the $F(LLD)$ curves and associated secondary cracking in fracture mechanics testing. Both phenomena arise from the anisotropy of the hot-rolled material described above. As the constraint in fracture mechanics specimens is higher than in SP specimens, the temperature range where load drop are observed, extends to higher temperature for the C(T) specimens (up to 100 °C versus up to -70°C in SP samples).

## 4.2 The meaning of orientation dependent ductile-to-brittle transition temperatures

The ductile-to-brittle transition temperatures $T_{CVN}$ recalculated from $T_{SP}$ give values in reasonable order of magnitude for the hot-extruded materials (all orientations) and for the hot-rolled material tested with S oriented samples, cf. Table 4. A direct comparison for the investigated materials is not possible, since Charpy or KLST based DBTTs are not available (except for the estimation for ODS-HR, Table 2). Nevertheless, KLST based DBTT values from the literature can be used for comparison (Table 5) to underpin this statement.

**Table 5**. Literature values for KLST based DBTTs of hot-rolled and hot-extruded ODS steels

| Material | Orientation | $T_{KLST}$ (°C) | $T_{CVN}$ (°C) * | Reference |
|---|---|---|---|---|
| 12Cr-ODS-HR Kobelco | LS | -104 | -39 | [21] |
| 12Cr-ODS-HR Kobelco | TS | -61 | 4 | [21] |
| 12Cr-ODS-HR Kobelco | TL | -4 | 61 | [21] |
| 12Cr-ODS-HR Kobelco | LT | -2 | 67 | [21] |
| 14Cr-ODS-HR CEA | LT | 14 | 79 | [29] |
| 14Cr-ODS-HR CEA | TL | 6 | 71 | [29] |
| 14Cr-ODS-HE CEA | LR | -95 | -30 | [29] |
| 14Cr-ODS-HE Getmat | LR | -54 | 11 | [30] |
| 14Cr-ODS-HE PSI | LR | 9 | 74 | [31] |
| 14Cr-ODS-HE PSI | RL | -7 | 58 | [31] |
| ODS-HR (this work) | LS | $\approx$ -70 | -5 | [22] |

* Recalculated from: $T_{CVN} = T_{KLST} + 65$ K

The only possible direct comparison of converted $T_{CVN}$ values from KLST and SP tests for ODS-HR shows a good agreement: -5 °C from KLST in orientation LS (Table 5) and -2 °C

from SP in orientation S (Table 4). As the correlation of orientations of KLST samples and SP samples is not straightforward [21], this good agreement should not be overrated. For the hot extruded materials, the effect of sample orientation is much smaller as compared to the hot-rolled material (Table 4).

In contrast, the SP tests with samples from ODS-HR in orientations L and T (where pop-ins occur at low test temperatures) give very high DBTTs (Table 4) which cannot be found in KLST based values (Table 5). The delamination-like defects in the weak zones of the material yield different fracture behaviours in KLST and SP samples. In case of LT or TL oriented KLST samples the delamination leads to secondary cracks and hence to a loss of constraint. This has a limited effect on the progression of the main crack. In LS or TS oriented KLST samples, the delamination leads to even higher energy absorption due to the deviation of the main crack [7,21]. In L or T oriented SP samples the weak zones are perpendicular to the in-plane tensile stresses which leads to failure at low loads [21]. Thus the effect of delamination is much more significant in SP specimens as compared to KLST/CVN specimens.

In conclusion, it is suggested that the correlation $T_{SP} = \alpha \cdot T_{CVN}$ can be applied for SP tests without pop-ins in the $F(v)$ curves. The negligence of existing pop-ins in the calculation of the energy is not an alternative as it makes the determination of a $T_{SP}$ value impossible (Fig. 10). Apart from that, the $T_{SP}$ values obtained from $F(v)$ with pop-ins are still useful for the comparison of different hot-rolled materials with respect to their susceptibility to delamination.

## 5. Conclusions

For the hot-rolled ODS steel, the pop-ins in the $F(v)$ curves were found to be associated with liftings (flakes) in the fracture surface. Such liftings were also observed in cases of pop-ins with $\Delta F/F_m < 0.1$. This finding is important, because a threshold of 0.1 is foreseen for the significance of pop-ins in the upcoming EN standard [25].

For the hot-rolled ODS steel, the occurrence of pop-ins in the SP $F(v)$ curves and associated flakes at the fracture surfaces corresponds with the susceptibility to secondary cracks in fracture mechanics testing. Both phenomena are caused by the anisotropy of the hot-rolled material and the existence of weak zones. They could not be observed in the hot-extruded materials.

The application of the established correlation between DBTTs from SP test and Charpy impact test ($T_{SP} = \alpha \cdot T_{CVN}$) is questionable for L/T oriented SP specimens of hot-rolled ODS material which exhibit pop-ins in the load-displacement curves. This is due to the different load situations of the weak zones in SP and KLST samples. In contrast, for S oriented SP samples the correlation is applicable. In hot-extruded ODS steels, the effect on anisotropy on the DBTT is significantly smaller as compared to hot-rolled materials. Therefore the correlation is applicable for hot-extruded ODS steels irrespective of the sample orientation.

## References

[1] R. Lindau, A. Möslang, M. Rieth, M. Klimiankou, E. Materna-Morris, A. Alamo, A.-A.F. Tavassoli, C. Cayron, A.-M. Lancha, P. Fernandez, N. Baluc, R. Schäublin, E. Diegele, G. Filacchioni, J.W. Rensman, B. v. d. Schaaf, E. Lucon, W. Dietz, Present development status of EUROFER and ODS-EUROFER for application in blanket concepts, Fusion Eng. Des. 75–79 (2005) 989–996. doi:10.1016/j.fusengdes.2005.06.186.

[2] R.L. Klueh, J.P. Shingledecker, R.W. Swindeman, D.T. Hoelzer, Oxide dispersion-strengthened steels: A comparison of some commercial and experimental alloys, J. Nucl. Mater. 341 (2005) 103–114. doi:10.1016/j.jnucmat.2005.01.017.

[3] D.A. McClintock, M.A. Sokolov, D.T. Hoelzer, R.K. Nanstad, Mechanical properties of irradiated ODS-EUROFER and nanocluster strengthened 14YWT, J. Nucl. Mater. 392 (2009) 353–359. doi:10.1016/j.jnucmat.2009.03.024.

[4] R. Lindau, A. Möslang, M. Schirra, P. Schlossmacher, M. Klimenkov, Mechanical and microstructural properties of a hipped RAFM ODS-steel, J. Nucl. Mater. 307–311, Part 1 (2002) 769–772. doi:10.1016/S0022-3115(02)01045-0.

[5] R. Chaouadi, G. Coen, E. Lucon, V. Massaut, Crack resistance behavior of ODS and standard 9%Cr-containing steels at high temperature, J. Nucl. Mater. 403 (2010) 15–18. doi:10.1016/j.jnucmat.2010.05.021.

[6] T.S. Byun, J.H. Yoon, S.H. Wee, D.T. Hoelzer, S.A. Maloy, Fracture behavior of 9Cr nanostructured ferritic alloy with improved fracture toughness, J. Nucl. Mater. 449 (2014) 39–48. doi:10.1016/j.jnucmat.2014.03.007.

[7] J. Chao, C. Capdevila, M. Serrano, A. Garcia-Junceda, J.A. Jimenez, G. Pimentel, E. Urones-Garrote, Notch Impact Behavior of Oxide-Dispersion-Strengthened (ODS) Fe20Cr5Al Alloy, Metall. Mater. Trans. A. 44 (2013) 4581–4594. doi:10.1007/s11661-013-1815-7.

[8] Y. Kimura, T. Inoue, F. Yin, K. Tsuzaki, Delamination Toughening of Ultrafine Grain Structure Steels Processed through Tempforming at Elevated Temperatures, ISIJ Int. 50 (2010) 152–161. doi:10.2355/isijinternational.50.152.

[9] A. Das, H.W. Viehrig, F. Bergner, C. Heintze, E. Altstadt, J. Hoffmann, Effect of microstructural anisotropy on fracture toughness of hot rolled 13Cr ODS steel – The role of primary and secondary cracking, J. Nucl. Mater. 491 (2017) 83–93. doi:10.1016/j.jnucmat.2017.04.059.

[10] A. Das, H.W. Viehrig, E. Altstadt, C. Heintze, J. Hoffmann, On the influence of microstructure on the fracture behaviour of hot extruded ferritic ODS steels, J. Nucl. Mater. 497 (2017) 60–75. doi:10.1016/j.jnucmat.2017.10.051.

[11] T. Misawa, T. Adachi, M. Saito, Y. Hamaguchi, Small punch tests for evaluating ductile-brittle transition behavior of irradiated ferritic steels, J. Nucl. Mater. 150 (1987) 194–202. doi:10.1016/0022-3115(87)90075-4.

[12] X. Mao, H. Takahashi, Development of a further-miniaturized specimen of 3 mm diameter for tem disk (ø 3 mm) small punch tests, J. Nucl. Mater. 150 (1987) 42–52. doi:10.1016/0022-3115(87)90092-4.

[13] X. Jia, Y. Dai, Small punch tests on martensitic/ferritic steels F82H, T91 and Optimax-A irradiated in SINQ Target-3, J. Nucl. Mater. 323 (2003) 360–367. doi:10.1016/j.jnucmat.2003.08.018.

[14] E. Fleury, J.S. Ha, Small punch tests to estimate the mechanical properties of steels for steam power plant: I. Mechanical strength, Int. J. Press. Vessels Pip. 75 (1998) 699–706. doi:10.1016/S0308-0161(98)00074-X.

[15] J. Kameda, X. Mao, Small-punch and TEM-disc testing techniques and their application to characterization of radiation damage, J. Mater. Sci. 27 (1992) 983–989. doi:10.1007/BF01197651.

[16] P. Dymáček, K. Milička, Creep small-punch testing and its numerical simulations, Mater. Sci. Eng. A. 510–511 (2009) 444–449. doi:10.1016/j.msea.2008.06.053.

[17] E. Altstadt, H.E. Ge, V. Kuksenko, M. Serrano, M. Houska, M. Lasan, M. Bruchhausen, J.-M. Lapetite, Y. Dai, Critical evaluation of the small punch test as a screening procedure for mechanical properties, J. Nucl. Mater. 472 (2016) 186–195. doi:10.1016/j.jnucmat.2015.07.029.

[18] E. Altstadt, M. Houska, I. Simonovski, M. Bruchhausen, S. Holmström, R. Lacalle, On the estimation of ultimate tensile stress from small punch testing, Int. J. Mech. Sci. 136 (2018) 85–93. doi:10.1016/j.ijmecsci.2017.12.016.

[19] J. Vivas, C. Capdevila, E. Altstadt, M. Houska, D. San-Martín, Importance of austenitization temperature and ausforming on creep strength in 9Cr ferritic/martensitic steel, Scr. Mater. 153 (2018) 14–18. doi:10.1016/j.scriptamat.2018.04.038.

[20] N. Okuda, R. Kasada, A. Kimura, Statistical evaluation of anisotropic fracture behavior of ODS ferritic steels by using small punch tests, J. Nucl. Mater. 386–388 (2009) 974–978. doi:10.1016/j.jnucmat.2008.12.265.

[21] E. Altstadt, M. Serrano, M. Houska, A. García-Junceda, Effect of anisotropic microstructure of a 12Cr-ODS steel on the fracture behaviour in the small punch test, Mater. Sci. Eng. A. 654 (2016) 309–316. doi:10.1016/j.msea.2015.12.055.

[22] J. Hoffmann, M. Rieth, L. Commin, S. Antusch, Microstructural anisotropy of ferritic ODS alloys after different production routes, Fusion Eng. Des. 98–99 (2015) 1986–1990. doi:10.1016/j.fusengdes.2015.05.002.

[23] I. Hilger, X. Boulnat, J. Hoffmann, C. Testani, F. Bergner, Y. De Carlan, F. Ferraro, A. Ulbricht, Fabrication and characterization of oxide dispersion strengthened (ODS) 14Cr steels consolidated by means of hot isostatic pressing, hot extrusion and spark plasma sintering, J. Nucl. Mater. 472 (2016) 206–214. doi:10.1016/j.jnucmat.2015.09.036.

[24] E.N. Klausnitzer, Micro-Specimens for Mechanical Testing, Materialprüfung. 33 (1991) 132–134.

[25] M. Bruchhausen, T. Austin, S. Holmström, E. Altstadt, P. Dymacek, S. Jeffs, R. Lancaster, R. Lacalle, K. Matocha, J. Petzová, European Standard on Small Punch Testing of Metallic Materials, in: ASME, 2017: p. V01AT01A065. doi:10.1115/PVP2017-65396.

[26] M. Bruchhausen, S. Holmström, J.-M. Lapetite, S. Ripplinger, On the determination of the ductile to brittle transition temperature from small punch tests on Grade 91 ferritic-martensitic steel, Int. J. Press. Vessels Pip. 155 (2017) 27–34. doi:10.1016/j.ijpvp.2017.06.008.

[27] P. Urwank, Unambiguous curve fitting and error estimation for charpy impact test data of reactor pressure vessel steels, suitable for a small number of samples, J. Nucl. Mater. 161 (1989) 24–29. doi:10.1016/0022-3115(89)90458-3.

[28] A. Das, H.-W. Viehrig, E. Altstadt, F. Bergner, J. Hoffmann, Why Do Secondary Cracks Preferentially Form in Hot-Rolled ODS Steels in Comparison with Hot-Extruded ODS Steels?, Crystals. 8 (2018) 306. doi:10.3390/cryst8080306.

[29] A.L. Rouffié, P. Wident, L. Ziolek, F. Delabrouille, B. Tanguy, J. Crépin, A. Pineau, V. Garat, B. Fournier, Influences of process parameters and microstructure on the fracture mechanisms of ODS steels, J. Nucl. Mater. 433 (2013) 108–115. doi:10.1016/j.jnucmat.2012.08.050.

[30] A. García-Junceda, M. Hernández-Mayoral, M. Serrano, Influence of the microstructure on the tensile and impact properties of a 14Cr ODS steel bar, Mater. Sci. Eng. A. 556 (2012) 696–703. doi:10.1016/j.msea.2012.07.051.

[31] Z. Oksiuta, P. Olier, Y. de Carlan, N. Baluc, Development and characterisation of a new ODS ferritic steel for fusion reactor application, J. Nucl. Mater. 393 (2009) 114–119. doi:10.1016/j.jnucmat.2009.05.013.

**Highlights**

- Small punch test results of 3 different ODS steels; comparison of hot-rolled vs. hot-extruded ODS
- In-depth analysis of load drops (pop-ins) in the force-displacement curves
- Analogy of secondary cracking in fracture mechanics testing and lifting (flakes) in SP fractures surfaces
- Evaluation of the empirical correlation between SP based and KLST based ductile-to-brittle transition temperatures for anisotropic materials